

DTP/96/48
June 1996

Observable jets from the BFKL chain

J. Kwiecinski^{a,b}, C. A. M. Lewis^{a,b} and A. D. Martin^b

^a Department of Theoretical Physics,
H. Niewodniczanski Inst. of Nuclear Physics,
ul. Radzikowskiego 152,
31-342 Krakow, Poland.

^b Department of Physics,
University of Durham,
Durham, DH1 3LE, UK.

Abstract

We derive a modified form of the BFKL equation which enables the structure of the gluon emissions to be studied in small x deep inelastic scattering. The equation incorporates the resummation of the virtual and unresolved real gluon emissions. We solve the equation to calculate the number of small x deep-inelastic events containing 0, 1, 2 ... resolved gluon jets, that is jets with transverse momenta $q_T > \mu$. We study the jet decomposition for different choices of the jet resolution parameter μ .

1. Introduction

The advent of the HERA electron-proton collider has opened up the possibility of testing QCD in the new and hitherto unexplored small x regime. The HERA measurements of the proton structure function $F_2(x, Q^2)$ show a striking rise with decreasing x , which with the latest data is now known with considerable precision [1, 2]. On the other hand from the theoretical point of view we know for sufficiently small x , such that $\alpha_S \ln 1/x \sim 1$, that it is necessary to resum the $(\alpha_S \ln 1/x)^n$ contributions in order to obtain reliable perturbative QCD predictions. At leading order this is accomplished by the Balitzkij, Fadin, Kuraev, Lipatov (BFKL) equation [3]. This equation effectively corresponds to the sum of gluon ladder diagrams of the type shown in Fig. 1 in which the transverse momenta q_T are unordered along the chain. This should be contrasted with DGLAP evolution where, in the leading $\ln Q^2$ approximation, the transverse momenta are strongly ordered from the hadronic to the hard scale Q^2 which in deep-inelastic lepton scattering is provided by the virtuality of the photon, namely

$$Q^2 \gg k_T^2 \gg k_{nT}^2 \gg \dots \quad (1)$$

Both BFKL and DGLAP evolution lead to an increase of the deep-inelastic scattering structure functions with decreasing x . In fact it is possible to obtain a satisfactory description of the rise of the structure function measured in the HERA small x regime using both approaches [4, 5, 6]. The inclusive nature of the structure function F_2 makes it extremely difficult, even with the precise HERA data, to use the observed x behaviour to reveal the underlying dynamics at small x . This is not surprising. The leading behaviour obtained from BFKL is an $x^{-\lambda}$ growth, whereas for DGLAP we anticipate an increase of the double logarithmic form $\exp(A[\ln(t/t_0) \ln(1/x)]^{\frac{1}{2}})$ where $t = \ln(Q^2/\Lambda^2)$. However, these are asymptotic predictions. For instance subleading $\ln 1/x$ effects will weaken the BFKL growth in the HERA regime [7, 8]. Moreover the DGLAP behaviour is dependent on the choice of a non-perturbative input form at some scale $Q^2 = Q_i^2$. It has been realized however, that the intimate relation between the increase of the cross sections with decreasing x and the absence of transverse momentum ordering, which is the basic property of the BFKL dynamics, should reflect itself in the properties of the final states in deep-inelastic lepton scattering. Indeed several dedicated measurements have been proposed and are being experimentally studied at HERA (see, for example, the reviews in ref. [9]).

The purpose of this paper is to study the detailed properties of the partonic final state produced by the gluon emissions along the BFKL chain. In this way we will gain insight into the BFKL equation, as well as detailing observables with which to probe the underlying small x dynamics. In particular we calculate the decomposition of the (total) deep-inelastic cross section into components $\sigma_n(\mu)$ which correspond to the production of a fixed number n of gluon jets each with transverse momentum $q_T > \mu$. That is we study the possible jet configurations in the central region between the current jet and the proton remnants. An interesting feature of BFKL dynamics is the possibility of producing jets even for $\mu > Q$. One of our aims is to quantify the yield of such jet configurations.

In the BFKL equation there is a delicate cancellation between the real gluon emissions and the virtual contributions. Clearly the cancellation is affected by the resolution $q_T > \mu$ that we impose. In particular we must ensure that the appropriate cancellation between the virtual contributions and the “unresolved” real gluon emissions with $q_T < \mu$ is maintained throughout the calculation. We must therefore first derive a modified form of the BFKL equation which will enable us to quantify the number of energetic *resolved* jets produced along the gluon chain, but in which the *virtual* and *unresolved* contributions are treated on an equal footing and are resummed. This is the subject of section 2. In section 3 we give an analytic solution for the resummation at low jet resolution, whereas in section 4 we consider more realistic values of the resolution μ and solve the modified BFKL equation by iteration to illustrate the jet decomposition of the BFKL gluon. At this stage it is still a theoretical study. In section 5 we use the BFKL gluon and the k_T -factorization theorem [10] to predict the jet decomposition of the observable structure function F_2 and the deep-inelastic cross section. Section 6 contains our conclusions.

2. The BFKL equation incorporating jet resolution $q_T > \mu$

In the small x regime the dominant parton is the gluon. Since we no longer have strong-ordering in transverse momenta along the gluon chain in Fig. 1 we must work in terms of the gluon distribution $f(x, k_T^2)$ unintegrated over its transverse momentum k_T . The relation of unintegrated distribution f to the conventional gluon distribution is

$$g(x, Q^2) = \int^{Q^2} \frac{dk_T^2}{k_T^2} f(x, k_T^2). \quad (2)$$

The unintegrated density f satisfies the BFKL equation which effectively sums up the leading $\alpha_S \ln 1/x$ contributions. In integral form it may be written [11, 12]

$$f(y, k_T^2) = f^{(0)}(y, k_T^2) + \bar{\alpha}_S \int_0^y dy' \int \frac{d^2 q_T}{\pi q_T^2} \left[\frac{k_T^2}{k_T'^2} f(y', k_T'^2) - f(y', k_T^2) \Theta(k_T^2 - q_T^2) \right], \quad (3)$$

with $\bar{\alpha}_S \equiv 3\alpha_S/\pi$. We have chosen to use the rapidity variable $y = \ln 1/x$ instead of x , and so the integral in (3) has come from the replacement

$$\int_x^1 \frac{dx'}{x'} \rightarrow \int_0^y dy'.$$

For convenience we have also introduced

$$k_T'^2 \equiv |\mathbf{q}_T + \mathbf{k}_T|^2. \quad (4)$$

Note that the dependence on $k_T'^2$ makes the angular integration in $d^2 q_T$ non-trivial. The inhomogeneous contribution $f^{(0)}$ in (3) corresponds to the “no-rung” contribution of Fig. 1. It is

the driving term of the equation and has to be input. We implicitly include under the d^2q_T integral in (3) the product of theta functions

$$\Theta(Q_f^2 - k_T'^2) \Theta(k_T'^2 - Q_0^2) \quad (5)$$

so that the emitted gluon is constrained to the domain $Q_0^2 < k_T'^2 < Q_f^2$. In the numerical predictions shown below we take $Q_0^2 = 1 \text{ GeV}^2$ and $Q_f^2 = 10^4 \text{ GeV}^2$.

Jet structure is embodied in the BFKL equation via real gluon emission from the gluon chain prior to its interaction with the photon probe (which takes place through the usual fusion subprocess $\gamma g \rightarrow q\bar{q}$). An observed jet is defined by a resolution parameter μ which specifies the minimum transverse momentum that must be carried by the emitted gluon for it to be detected. For realistic observed jets in the experiments at HERA, the lowest reasonable choice for the resolution cut-off parameter μ appears to be about $\mu = 3.5 \text{ GeV}$. However, we also present results for $\mu = 6 \text{ GeV}$ and, so as to gain theoretical insight, for the low values of $\mu = 1$ and 2 GeV .

If an emitted gluon has transverse momentum $q_T < \mu$ then the radiation is said to be unresolved. The unresolved radiation must be treated at the same level as the virtual corrections to ensure that the singularities as $q_T^2 \rightarrow 0$ cancel in the q_T^2 integration. To do this we first rewrite the BFKL equation (3) in the symbolic form

$$f = f^{(0)} + \int_0^y dy' K \otimes f(y'), \quad (6)$$

where \otimes denotes the convolution over q_T . We divide the real gluon emission contribution into resolved and unresolved parts using the identity

$$\Theta(q_T^2 - \mu^2) + \Theta(\mu^2 - q_T^2) = 1, \quad (7)$$

where the first term denotes the real resolved emission and the second the real unresolved emission. We then combine the unresolved component with the virtual contribution [13]. That is

$$f = f^{(0)} + \int_0^y dy' (K_R + K_{UV}) \otimes f(y'), \quad (8)$$

where the kernel K_R for the *resolved* emissions with $q_T > \mu$ is given by

$$K_R \otimes f(y') = \bar{\alpha}_S(k_T^2) k_T^2 \int \frac{d^2q_T}{\pi q_T^2} \Theta(q_T^2 - \mu^2) \frac{1}{k_T'^2} f(y', k_T'^2), \quad (9)$$

while K_{UV} , the combined *unresolved* and *virtual* part of the kernel, satisfies

$$K_{UV} \otimes f(y') = \bar{\alpha}_S(k_T^2) \int \frac{d^2q_T}{\pi q_T^2} \left[\frac{k_T^2}{k_T'^2} f(y', k_T'^2) \Theta(\mu^2 - q_T^2) - f(y', k_T^2) \Theta(k_T^2 - q_T^2) \right], \quad (10)$$

with $k_T'^2 \equiv |\mathbf{q}_T + \mathbf{k}_T|^2$. These identifications of the kernels follow by comparing (8) with (3). The $q_T^2 \rightarrow 0$ singularity is now cancelled between the unresolved and virtual contributions, and by working with the combined kernel K_{UV} we will ensure that the cancellation remains intact.

We seek a BFKL equation for the real resolved emissions in which the unresolved and virtual contributions have been resummed. To do this we write the BFKL equation (8) in the differential form

$$\frac{\partial f}{\partial y} = \left(\frac{\partial f^{(0)}}{\partial y} + K_R \otimes f \right) + K_{UV} \otimes f, \quad (11)$$

and treat the expression in brackets as the inhomogeneous contribution. We solve the inhomogeneous equation in the standard way. We first find a solution to the homogeneous equation and then we obtain the full solution via an integrating factor. The homogeneous version of (11) is

$$\frac{\partial \Delta}{\partial y} = K_{UV} \otimes \Delta \quad (12)$$

with solution

$$\Delta(y) = \exp(y K_{UV}), \quad (13)$$

and so the integrating factor is $\Delta^{-1} = \exp(-y K_{UV})$. Hence the full solution of (11) is

$$\begin{aligned} f(y) &= \int_0^y dy' \Delta(y) \otimes \Delta^{-1}(y') \otimes \left(\frac{\partial f^{(0)}}{\partial y'} + K_R \otimes f(y') \right) \\ &= \int_0^y dy' e^{(y-y')K_{UV}} \otimes \left(\frac{\partial f^{(0)}}{\partial y'} + K_R \otimes f(y') \right). \end{aligned} \quad (14)$$

Thus we have derived a BFKL equation for the gluon distribution f in which the unresolved and virtual terms have been resummed in the exponential factor. The equation is of the form

$$f(y) = \hat{f}^{(0)}(y) + \int_0^y dy' \hat{K} \otimes f(y') \quad (15)$$

where the driving term has become

$$\hat{f}^{(0)}(y) = \int_0^y dy' e^{(y-y')K_{UV}} \otimes \frac{\partial f^{(0)}}{\partial y'} \quad (16)$$

and the new kernel

$$\hat{K} = e^{(y-y')K_{UV}} \otimes K_R. \quad (17)$$

Recall that the original BFKL kernel, $K_R + K_{UV}$, has no y (i.e. x) dependence. However, upon the resummation of the unresolved and virtual radiation we generate an explicit y dependence. In fact the kernel \hat{K} of (15) is a function of only the difference $y - y'$ (i.e. of $\ln x'/x$) and not y and y' individually, see (17).

3. Analytical solution at low μ

In section 4 we numerically solve the modified BFKL equation for $f(y, k_T^2)$ and, by iteration, determine the probability of the emission of n gluon jets with $q_T > \mu$. However, first it is informative to derive an approximate form of the above equation which holds in the (theoretical)

limit of small μ^2/k_T^2 . In this limit it is possible to resum the unresolved and virtual contributions in a closed analytic form. The crucial observation is that for small μ^2/k_T^2 we may write

$$k_T'^2 \equiv |\mathbf{q}_T + \mathbf{k}_T|^2 \approx k_T^2$$

in the integrand for the unresolved real emission term in (10). Then (10) simplifies to become

$$\begin{aligned} K_{UV} \otimes f(y') &= \bar{\alpha}_S(k_T^2) f(y') \int \frac{dq_T^2}{q_T^2} [\Theta(\mu^2 - q_T^2) - \Theta(k_T^2 - q_T^2)] + \mathcal{O}\left(\frac{\mu^2}{k_T^2}\right) \\ &= -\bar{\alpha}_S(k_T^2) \ln\left(\frac{k_T^2}{\mu^2}\right) f(y') + \mathcal{O}\left(\frac{\mu^2}{k_T^2}\right). \end{aligned} \quad (18)$$

Thus the homogeneous solution of the BFKL equation (11) is

$$\Delta(y) = \exp(y K_{UV}) = \exp\left(-y \bar{\alpha}_S(k_T^2) \ln(k_T^2/\mu^2)\right), \quad (19)$$

that is the resummation is given by a simple analytic form. As a consequence, in the small μ limit, the modified BFKL equation (15) becomes

$$f(y, k_T^2) = \hat{f}^{(0)}(y, k_T^2) + \bar{\alpha}_S(k_T^2) \int_0^y dy' \Delta(y - y', k_T^2) \int \frac{d^2 q_T}{\pi q_T^2} \Theta(q_T^2 - \mu^2) \frac{k_T^2}{k_T'^2} f(y', k_T'^2) \quad (20)$$

where here $k_T'^2 = |\mathbf{q}_T + \mathbf{k}_T|^2$, and the driving term is given by

$$\hat{f}^{(0)}(y, k_T^2) = \int_0^y dy' \Delta(y - y', k_T^2) \frac{\partial f^{(0)}(y', k_T^2)}{\partial y'}. \quad (21)$$

Of course for the results presented below we do not use the low μ approximation, although to gain insight we will compare the full prediction of (16) for $\hat{f}^{(0)}$ with the approximate $\mathcal{O}(\mu^2/k_T^2)$ result given in (21).

4. Jet decomposition of the BFKL gluon

The BFKL equation was expressed in form (15) specifically so that we can decompose the unintegrated gluon distribution f into the sum of contributions with different numbers of *resolved* gluon jets with transverse momenta $q_T > \mu$. That is

$$f(y) = \sum_{n=0}^{\infty} f^n(y) \quad (22)$$

where f^n denotes the contribution to the unintegrated gluon distribution f arising from n resolved jets in the chain, each with $q_T > \mu$, see Fig. 2. The n -jet contribution f^n obviously depends on the resolution μ , whereas the sum f does not. Using (15) we have

$$f^n(y) = \int_0^y dy' \hat{K} \otimes f^{n-1}(y') \quad (23)$$

where the 0-jet contribution $f^0 = \hat{f}^{(0)}$ of (16) and where \hat{K} is the full resummed kernel of (17). For the initial non-perturbative input $f^{(0)}$ in (16) we take

$$f^{(0)}(y) = 3N(1 - e^{-y})^5 \exp(-k_T^2/Q_0^2) \quad (24)$$

where the normalization N is fixed so that the gluon, integrated over the region $k_T^2 > Q_0^2$, carries half the momentum of the proton. We set $Q_0^2 = 1 \text{ GeV}^2$.

Although the sum $f(y)$ of (22) is independent of μ , the individual contributions $f^n(y)$ are μ dependent. Recall that \otimes stands for an integration over d^2q_T (see (9) and (10)), and that f is a function of k_T^2 as well as y . In Figs. 3, 4 and 5 we show the decomposition of $f(y, k_T^2)$ for $k_T = 2, 5$ and 10 GeV respectively, in each case taking three different values for the resolution, namely $\mu = 1, 2$ and 3.5 GeV . The gluon density, and its decomposition, are not observable directly. The choices we have made for μ are, at this stage, solely to gain insight into the structure of the BFKL gluon. The results show the following features:

- (i) Gluon jets with $\mu > k_T$ occur; the probability increases as x decreases.
- (ii) The lower the value of μ , the greater the number of resolved jets, that is the greater the preponderance of multijet configurations.
- (iii) As x decreases, the greater the diffusion in $\ln q_T^2$ so that an n -jet configuration first increases in probability and then decreases as higher jet-configurations take over.
- (iv) The higher the value of k_T^2 the sooner in x (as x decreases) will a given multijet configuration go through this rise and fall.
- (v) As k_T^2/μ^2 increases the 0-jet contribution drops rapidly to zero.

The results for low values of the resolution parameter μ show that the functions f_n have a maximum which shifts to smaller values of x with increasing n . This maximum is a straightforward consequence of virtual corrections which, for low μ , are not entirely compensated by (unresolved) real radiation. The maximum disappears for large μ and we have this structure for all values of k_T .

Some insight into the behaviour can be obtained from the analytic form presented in section 3, which applies when μ^2/k_T^2 is small. In this limit the virtual and unresolved real terms lead to a suppression factor

$$\Delta(y) = e^{-Ay} \quad (25)$$

where $A \equiv \bar{\alpha}_S \ln(k_T^2/\mu^2)$. Thus from (21) we obtain the 0-jet contribution

$$f^0 = \hat{f}^{(0)}(y, k_T^2) = e^{-Ay} \int_0^y dy' e^{Ay'} 3N e^{-k_T^2/Q_0^2} \frac{d}{dy'} (1 - e^{-y'})^5, \quad (26)$$

that is the k_T dependence of f^0 is essentially the same as the k_T dependence of the driving term $f^{(0)}$ of (24). This explains the origin of feature (v), that the 0-jet contribution falls

rapidly to zero with increasing k_T^2 . Fig. 6 compares the analytic approximation with the full result for $\mu^2 = 1 \text{ GeV}^2$ and $k_T^2 = 4 \text{ GeV}^2$. We see that the analytic form reproduces the shape of the numerical solution, but fails in the normalization. Also the peak in the numerical prediction shifts slightly to smaller x . Thus the analytical approximation cannot be used as a valid representation for the jet contributions, even for a resolution as low as 1 GeV^2 .

5. Jet decomposition of $F_i(x, Q^2)$ at small x

We are now in a position to estimate the probability of the different multijet configurations in the small x observables that are driven by the BFKL gluon. The most relevant process to study is deep-inelastic scattering at HERA. Using the results of section 4, we calculate the jet decomposition of the proton structure functions $F_i(x, Q^2)$. In other words we determine what fraction of events that make up the inclusive measurement of $F_i(x, Q^2)$ contain no-jets, one jet, two jets etc. as a function of x, Q^2 and the jet resolution parameter μ . Recall that our jets are gluons emitted with transverse momentum $q_T > \mu$.

From knowledge of the BFKL gluon f we can determine the behaviour of the structure functions via the k_T factorization theorem, see Fig. 2. For the transverse and longitudinal functions we have

$$F_{T,L}(x, Q^2) = \int_x^1 \frac{dx'}{x'} \int \frac{dk_T^2}{k_T^4} f\left(\frac{x}{x'}, k_T^2\right) F_{T,L}^{\gamma g}(x', k_T^2, Q^2) \quad (27)$$

where, to lowest order, photon-gluon fusion $F^{\gamma g}$ is given by the quark box (and crossed box) contributions, as shown in Fig. 7. To carry out the integration over the quark line in Fig. 7 we express its four momenta κ in terms of the Sudakov variables

$$\kappa = \alpha p - \beta q' + \kappa_T$$

where $q' = q + xp$ and p are the basic light-like momenta (q and p are the 4-momenta of the virtual photon and proton respectively). The variable α is fixed by the quark mass-shell constraint, leaving integrations over β and κ_T . Evaluating the box contributions, equation (27) then becomes [14]

$$\begin{aligned} F_T(x, Q^2) &= 2 \sum_q e_q^2 \frac{Q^2}{4\pi} \int_{k_0^2} \frac{dk_T^2}{k_T^4} \int_0^1 d\beta \int d^2 \kappa'_T \alpha_S f\left(\frac{x}{x'}, k_T^2\right) \\ &\times \left\{ \left[\beta^2 + (1-\beta)^2 \right] \left[\frac{\kappa_T^2}{D_1^2} - \frac{\kappa_T \cdot (\kappa_T - \kappa_T)}{D_1 D_2} \right] + \frac{m_q^2}{D_1^2} - \frac{m_q^2}{D_1 D_2} \right\} \end{aligned} \quad (28)$$

$$\begin{aligned} F_L(x, Q^2) &= 2 \sum_q e_q^2 \frac{Q^4}{4\pi} \int_{k_0^2} \frac{dk_T^2}{k_T^4} \int_0^1 d\beta \beta^2 (1-\beta)^2 \int d^2 \kappa'_T \\ &\times \alpha_S f\left(\frac{x}{x'}, k_T^2\right) \left\{ \frac{1}{D_1^2} - \frac{1}{D_1 D_2} \right\} \end{aligned} \quad (29)$$

where the denominators

$$\begin{aligned} D_1 &= \kappa_T^2 + \beta(1-\beta)Q^2 + m_q^2 \\ D_2 &= |\kappa_T - \mathbf{k}_T|^2 + \beta(1-\beta)Q^2 + m_q^2 \end{aligned}$$

and where $\kappa'_T = \kappa_T - (1-\beta)k_T$. The x' integration of (27) is implicit in the $d^2\kappa'_T$ and $d\beta$ integrations. Indeed x' is fixed in terms of κ'_T and β

$$x' = \left[1 + \frac{\kappa_T'^2 + m_q^2}{\beta(1-\beta)Q^2} + \frac{k_T^2}{Q^2} \right]^{-1}, \quad (30)$$

which ensures that the requirement $0 < x' < 1$ is satisfied. Of course the integration regions of (28) and (29) must be constrained by the condition

$$x'(\beta, \kappa_T'^2, k_T^2, Q^2) > x \quad (31)$$

so that the argument $z = x/x'$ of f satisfies the requirement $z < 1$. In (28) and (29) we sum over the quark flavours; we take the masses to be $m_q = 0$ for u, d, s quarks and $m_c = 1.5$ GeV for the charm quark. The argument of α_S is taken to be $\kappa_T'^2 + m_0^2$, which allows integration over the entire region of $\kappa_T'^2$. For the light quarks we take $m_0 = 1$ GeV 2 ; the results are not very sensitive to variations of m_0 about this value. For the charm quark contribution we set $m_0^2 = m_c^2$. Also we set $k_0^2 = 1$ GeV 2 .

The jet decomposition of $F_{L,T}$ are simply obtained by substituting the n -jet unintegrated distribution f^n into (28) and (29). In this way we can break down the observables into their component n -jet contributions, for example for $F_2 = F_L + F_T$ we have

$$F_2 = \sum_{n=0}^{\infty} F_2^n. \quad (32)$$

Figs. 8 and 9 show the components $F_2^n(x, Q^2)$ for deep inelastic events containing n observed jets, where in the upper plot we require the jets to have $q_T > 3.5$ GeV, whereas in the lower plot we demand $q_T > 6$ GeV. Figs. 8 and 9 correspond to $Q^2 = 10$ and 20 GeV 2 respectively. For these choices of jet resolution it can be seen that the 0-jet configuration dominates. That is most of the emission from the BFKL ladder is in the form of unresolved and virtual gluon radiation. As expected the n -jet configurations first become important (with decreasing x) for the lower resolution, $\mu = 3.5$ GeV, and the higher Q^2 value, $Q^2 = 20$ GeV 2 , and begin to compete with the 0-jet rate for $x \lesssim 10^{-5}$. In fact the 4-jet rate becomes comparable with the 0-jet rate for $x \sim 10^{-6}$.

Although the 0-jet configuration dominates in the HERA kinematic regime, there is still a non-negligible contribution from resolved jets. For example, at $Q^2 = 10$ GeV 2 and $x = 2 \times 10^{-4}$ the 1 and 2 jet contributions are each approximately $\frac{1}{3}$ of the 0-jet rate, and even the 3 and 4 jet configurations occur at a reasonable rate. Also notice the production of resolvable jets with $\mu^2 \gtrsim Q^2$ is important — this is a straightforward consequence of diffusion in k_T^2 .

The experiments at HERA show that the (inclusive) structure function F_2 rises as x decreases. How is this rise made up from the various multijet configurations? First we look at the results for the lower jet resolution, $\mu = 3.5$ GeV. Although the 0-jet rate dominates, its increase with decreasing x is relatively weak compared to the data. The rise of F_2 comes from the increasing importance of the higher jet configurations. On the other hand at the higher resolution, $\mu = 6$ GeV, the 0-jet configuration is even more dominant and shows a steeper rise over the same x range, as is required for consistency of the results. This characteristic difference should hopefully be seen in the measurement of the individual jet structure functions.

The cross section for deep-inelastic scattering is readily calculated from $F_{T,L}$. We have

$$\sigma = 4\pi\alpha^2 \int \frac{dx}{x} \int \frac{dQ^2}{Q^4} \left\{ y^2 x F_1(x, Q^2) + (1-y) F_2(x, Q^2) \right\} \quad (33)$$

where as usual $y = Q^2/xs$, $F_T = 2xF_1$ and $F_L = F_2 - 2xF_1$. Here we present results for the component cross sections σ^n for deep-inelastic events containing n jets with $q_T > \mu$, again for two choices of resolution $\mu = 3.5$ and 6 GeV. We take $\sqrt{s} = 300$ GeV and integrate σ over the interval $0.01 < y < 0.5$ so as to approximately reproduce the HERA domain. Figs. 10, 11, 12 and 13 show respectively the 0, 1, 2 and 3 jet cross sections integrated over x and Q^2 bins of size $\Delta x = 2 \times 10^{-4}$ and $\Delta Q^2 = 10$ GeV 2 , where the two entries in each bin correspond to a gluon jet with resolution $\mu = 3.5$ and 6 GeV respectively. We see that there are an appreciable number of identifiable jets. For example, if we take a resolved jet to be one with $q_T > 3.5$ GeV and an integrated luminosity $\mathcal{L} = 10$ pb $^{-1}$, then in the bin defined by $0.8 \times 10^{-3} < x < 10^{-3}$ and $15 < Q^2 < 25$ GeV 2 we predict 1052, 790, 392 events containing 1, 2, 3 jets as compared to 6790 events with no identifiable jet.

Recall that the predictions are obtained by numerically solving the BFKL equation for the gluon. The normalisation is dependent of the choice of the cut-off. Here we have taken the cut-off to be 1 GeV 2 , which was found to give a satisfactory description of the inclusive F_2 distribution. However, the fraction of events containing 0, 1, 2, ... identifiable gluon jets is independent of the choice of the cut-off. For example, for the above $(\Delta x, \Delta Q^2)$ bin and for the lower jet resolution of $\mu = 3.5$ GeV we find 75% of the cross section contains no observable jet and that 1, 2 and 3 jets occur 11, 8, 4% of the time respectively. Only 2% of the events contain more than 3 jets. For the higher jet resolution of $\mu = 6$ GeV we predict that the BFKL chain will give 90% of the events with no observable jet, leaving only 10% of the total to be split between 1, 2, ... jet events.

We see from Figs. 11 and 12 that the 2-jet rate is comparable to the 1-jet rate, and moreover that the 2-jet/1-jet ratio increases with increasing resolution μ . This type of behaviour is consistent with the expectations of the conservation of transverse momentum.

6. Summary and Conclusions

In this paper we have formulated a modified form of the BFKL equation which allows an exclusive analysis of the multijet yields in deep-inelastic lepton scattering in the small x regime. The jets are defined as gluon emissions from the BFKL chain which have transverse momenta q_T greater than a specified resolution μ . We first solved the modified BFKL equation to determine the jet decomposition of the unintegrated gluon distribution $f(x, k_T^2)$. We then used the k_T -factorization theorem to determine the jet decomposition of the structure function $F_2(x, Q^2)$ and of the total deep-inelastic cross section in the HERA small x regime. We presented the jet decompositions as a function of the kinematic variables and for different choices of the jet resolution parameter μ .

The modified BFKL equation is shown symbolically in (15) and the kernel \hat{K} in (17). The equation embodies a resummation of the virtual contributions together with the *unresolved* real gluon emissions with $q_T < \mu$. As a consequence the kernel \hat{K} has an explicit $y = \ln 1/x$ dependence, which depends on the amount of unresolved radiation and so is a function of μ . Indeed for unrealistically low values of μ we derived, for pedagogic purposes, the analytic form of the y dependence of the kernel, see (19). For the more realistic numerical solutions that we present the correlation between the x dependence of the n -jet cross sections and the resolution parameter μ is apparent.

The behaviour of the n -jet contribution to the gluon f , or to F_2 , exhibits a characteristic behaviour as x decreases, rising to a maximum and then falling back to zero. The higher the value of n the lower the value of x at which the maximum occurs. In the HERA small x regime the behaviour is only apparent for low choices of the parameter μ , for example $\mu \sim 1$ GeV, see Figs. 3, 4 and 5. For experimentally realistic values of the resolution parameter (say $\mu = 3.5$ or 6 GeV) the maxima shift to very small values of x . The dominant contribution in the HERA range then comes from events with no resolved gluon jets emitted from the BFKL chain. Nevertheless the 1, 2, 3, ...jet rates are still significant. An interesting feature of the multijet cross sections is that they are non-negligible even if $\mu > Q$. The existence of such jets with $q_T > Q$ is a straightforward consequence of the characteristic $\ln k_T^2$ diffusion along the BFKL gluon chain.

To sum up, we have made an exploratory study of a form of the BFKL equation which allows the final state jet configurations to be determined in a consistent manner. We solved the equation and presented sample results to illustrate the properties of these gluon jets which occur in deep inelastic scattering at small x as a result of BFKL dynamics. Of course there are subleading $\ln 1/x$ and fixed-order QCD jet contributions to consider. These may modify the predictions in the HERA regime, but with decreasing x the BFKL behaviour should become increasingly dominant. One non-leading effect is the imposition of the constraint $q_{nT}^2 < x_n k_T^2 / x$ (in the notation of Fig. 1) which follows from the requirement that the virtuality of the gluon links is dominated by $-k_T^2$ [7, 8]. If this were done we find that it would limit the available phase space for multijet production and, as a consequence, reduce the yield of multijet events.

Acknowledgements

J.K. thanks the Department of Physics and Grey College of the University of Durham, and C.A.M.L. thanks the H. Niewodniczanski Institute of Nuclear Physics in Krakow, for their warm hospitality, and thanks the UK Particle Physics and Astronomy Research Council for a Studentship. This work has been supported in part by Polish KBN grant no. 2 P03B 231 08 and the EU under contracts nos. CHRX-CT92-0004 and CHRX-CT93-0357.

Appendix: Numerical techniques used to solve the BFKL equation

Here we briefly describe the numerical method that we used to solve the BFKL equation (15). The starting point is the Chebyshev polynomial expansion of the unintegrated gluon distribution $f(y, k_T^2)$ in which we map the region $Q_0^2 < k_T^2 < Q_f^2$ into the interval $(-1, 1)$ in terms of the variable τ defined by

$$\tau(k_T^2) = 2 \ln \left(\frac{k_T^2}{Q_f Q_0} \right) \Big/ \ln \left(\frac{Q_f^2}{Q_0^2} \right). \quad (\text{A1})$$

We expand the gluon distribution f in the polynomial form

$$f(y, k_T^2) = \sum_{i=1}^N C_i \left(\tau(k_T^2) \right) f_i(y) \quad (\text{A2})$$

where $f_i(y)$ are the values of $f(y, k_T^2)$ at the $(k_T^2)_i$ nodes obtained from

$$\frac{(k_T^2)_i}{Q_f Q_0} = \left(\frac{Q_f}{Q_0} \right)^{\tau_i}, \quad (\text{A3})$$

with τ_i defined by

$$\tau_i = \cos[(i - \frac{1}{2})\pi/N], \quad (\text{A4})$$

and N the number of terms in the Chebyshev polynomial. The k_T^2 dependent functions C_i are obtained from the Chebyshev polynomial functions

$$T_n(\tau) = \cos(n \arccos(\tau)) \quad (\text{A5})$$

and are given by

$$C_i(\tau) = \frac{2}{N} \sum_{n=1}^N \nu_n T_n(\tau) T_n(\tau_i), \quad (\text{A6})$$

where $\nu_n = 1$ for $n > 1$, and $\nu_1 = \frac{1}{2}$. A good approximation for the k_T^2 dependence of f is obtained with typically $N = 20$.

The expansion (A2) is then substituted into the BFKL equation (15) to give the discretised (symbolic) form

$$f_i(y) = f_i^{(0)}(y) + \int_0^y dy' \sum_{i=1}^N \hat{K}_{i,k}(y - y') f_k(y'), \quad (\text{A7})$$

where the full kernel (17) now becomes

$$\hat{K}_{i,k} = \sum_l [e^{(y-y')K_{UV}}]_{i,l} K_{l,k}^R \quad (\text{A8})$$

and the input distribution $\hat{f}_i^{(0)}(y)$ of (16) is

$$f_i^{(0)}(y) = \int_0^y dy' \sum_k [e^{(y-y')K_{UV}}]_{i,k} \frac{\partial f_k^{(0)}(y')}{\partial y'}. \quad (\text{A9})$$

The substitution of (A2) into (7) and (8) gives the explicit form of the kernels K_R and K_{UV} respectively. The BFKL equation (A7) is a Volterra-type integral equation, which we solve iteratively for the $f_i(y)$'s. The gluon distribution $f(y, k_T^2)$ is then reconstructed from (A2).

We also use a Chebyshev interpolation to calculate the $Y \equiv y - y'$ dependence of the matrix elements of exponential matrix in (A8) and (A9). For convenience we denote the matrix elements

$$[e^{Y K_{UV}}]_{i,k} \equiv M(Y)_{i,k}. \quad (\text{A10})$$

As before we expand in terms of Chebyshev polynomials

$$M(Y)_{i,k} = \sum_{j=1}^J C_j(\tau(Y)) M_{i,k}^j \quad (\text{A11})$$

where M^j are the values of $M(Y)$ at the nodes Y_j . Here we take $J = 10$. We map the relevant region $0 < Y < Y_{\max}$, where $Y_{\max} = \log(1/X_{\min})$, into the interval $-1 < \tau < 1$ by choosing

$$\tau(Y) = (2Y - Y_{\max})/Y_{\max}. \quad (\text{A12})$$

The C_j is given by (A6) (together with (A4) and (A5)) with i replaced by j . It remains to calculate $M(Y)$ at the nodes $Y = Y_j$. We do this by solving

$$\frac{\partial M_{i,k}(Y)}{\partial y} = \sum_{j=1}^J (K_{UV})_{i,j} M_{j,k}(Y). \quad (\text{A13})$$

using the Runge-Kutta method with the boundary condition $M_{i,k}(Y = 0) = I_{i,k}$.

References

- [1] H1 collaboration: S. Aid *et al.*, DESY report 96-039, Z. Phys. **C** (in press).
- [2] ZEUS collaboration: M. Derrick *et al.*, Z. Phys. **C69** (1996) 607, DESY report 96-076, Z. Phys. **C** (in press).
- [3] E.A. Kuraev, L.N. Lipatov and V.S. Fadin, Phys. Lett. **B60** (1975) 50; Sov. Phys. JETP **44** (1976) 443; Sov. Phys. JETP **45** (1977) 199.
Ya. Ya. Balitsky and L.N. Lipatov, Sov. J. Nucl. Phys. **28** (1978) 822.
- [4] A.D. Martin, R.G. Roberts and W.J. Stirling, Phys. Rev. **D50** (1994) 6734; Phys. Lett. **354** (1995) 155.
- [5] M. Glück, E. Reya and A. Vogt, Z.Phys. **C67** (1995) 433.
- [6] J. Kwieciński, A.D.Martin and P.J. Sutton, Phys. Rev. **D53** (1996) 6094.
- [7] J. Kwieciński, A.D. Martin, P.J. Sutton, Durham preprint DTP/96/02 (Z.Phys. **C**, in print).
- [8] B. Andersson, G. Gustafson and J. Samuelsson, Lund preprint LU TP 95-13.
- [9] J. Kwieciński, Nucl. Phys. **B**, Proc. Suppl. **39 BC** (1995) 58;
M. Kuhlen, Proc. of DIS95 Workshop, Paris 1995, eds. J.F. Laporte and Y. Sirois, p.345.
- [10] S. Catani, M. Ciafaloni and F. Hautmann, Phys. Lett. **B242** (1990) 97; Nucl. Phys. **B366** (1991) 657;
J.C. Collins and R.K. Ellis, Phys. Lett. **B360** (1991) 3;
E.M. Levin, M.G. Ryskin and A.G. Shuvaev, Sov. J. Nucl. Phys. **53** (1991) 657.
- [11] M. Ciafaloni, Nucl. Phys. **B296** (1988) 49.
- [12] S. Catani, F. Fiorani and G. Marchesini, Phys. Lett. **B234** (1990) 339; Nucl. Phys. **B336** (1990) 18;
- [13] T. Jaroszewicz, Acta. Phys. Polon. **B11** (1980) 965.
- [14] A.J. Askew, J. Kwieciński, A.D. Martin and P.J. Sutton, Phys. Rev. **D47** (1993) 3775.

Figure Captions

Fig. 1 The unintegrated gluon distribution, $f(x, k_T^2)$, is effectively the sum of the ladder diagrams formed by the modulus squared of such amplitudes. The leading $\alpha_S \ln 1/x$ resummation is accomplished by the BFKL equation.

Fig. 2 The modulus squared of this diagram gives the component F_i^n of the proton structure function F_i which arises from the contribution f^n to the gluon distribution f in which there are n *resolved* gluon jets emitted along the BFKL chain, that is n gluons with $q_T > \mu$. The black circles are to indicate the presence of both virtual and unresolved gluon emissions. The component F_i^n is calculated by the k_T -factorization theorem, which has the symbolic form $F_i^n = F_i^{\gamma g} \otimes f^n$, see (27) and (32).

Fig. 3 The n -jet contributions to the unintegrated gluon distribution $f(x, k_T^2)$ for three different values of the jet resolution parameter μ and for $k_T = 2$ GeV.

Fig. 4 The same as Fig. 2 but for $k_T = 5$ GeV.

Fig. 5 The same as Fig. 2 but for $k_T = 10$ GeV.

Fig. 6 The comparison of the analytic and numerical solutions for the 0-jet contribution $f^0(x, k_T^2)$ to the unintegrated gluon distribution.

Fig. 7 The quark box and crossed box diagrams describing photon-gluon fusion, $F^{\gamma g}$ in (27).

Fig. 8 The decomposition of the proton structure function $F_2(x, Q^2)$ into contributions coming from different numbers of resolved gluon jets for experimentally accessible values of the resolution parameter $\mu = 3.5$ and 6 GeV. The decomposition is shown as a function of x for $Q^2 = 10$ GeV 2 .

Fig. 9 The same as Fig. 8 but for $Q^2 = 20$ GeV 2 .

Fig. 10 The cross-section (in pb) for deep-inelastic scattering in which there are no resolved gluon jets shown in different x, Q^2 bins in the region accessible at HERA. The width of the bins are $\Delta Q^2 = 10$ GeV 2 and $\Delta x = 2 \times 10^{-4}$. The upper and lower values correspond to the resolution parameter $\mu = 3.5$ and 6 GeV respectively.

Fig. 11 The same as Fig. 10 but from the contribution in which there is one, and only one, gluon resolved jet with $q_T > \mu$.

Fig. 12 The same as Fig. 10 but for two resolved gluon jets.

Fig. 13 The same as Fig. 10 but for three resolved gluon jets.

fig. 1

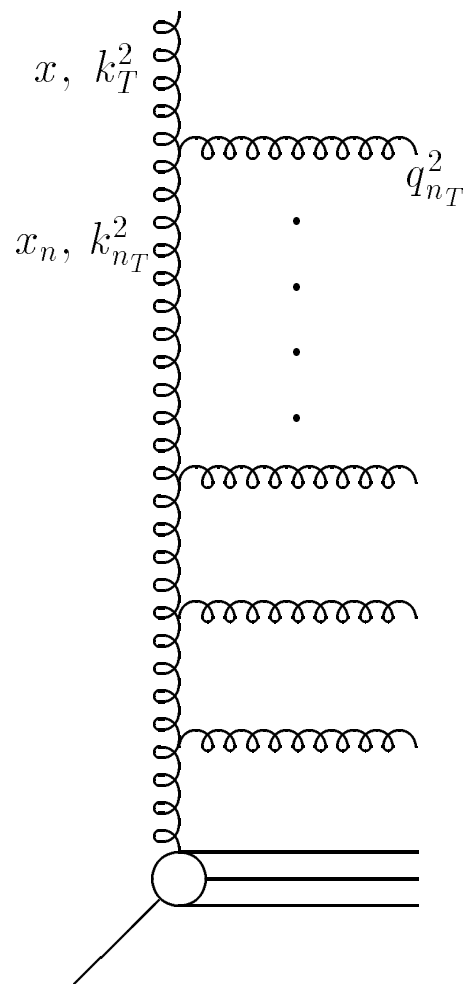


fig. 2

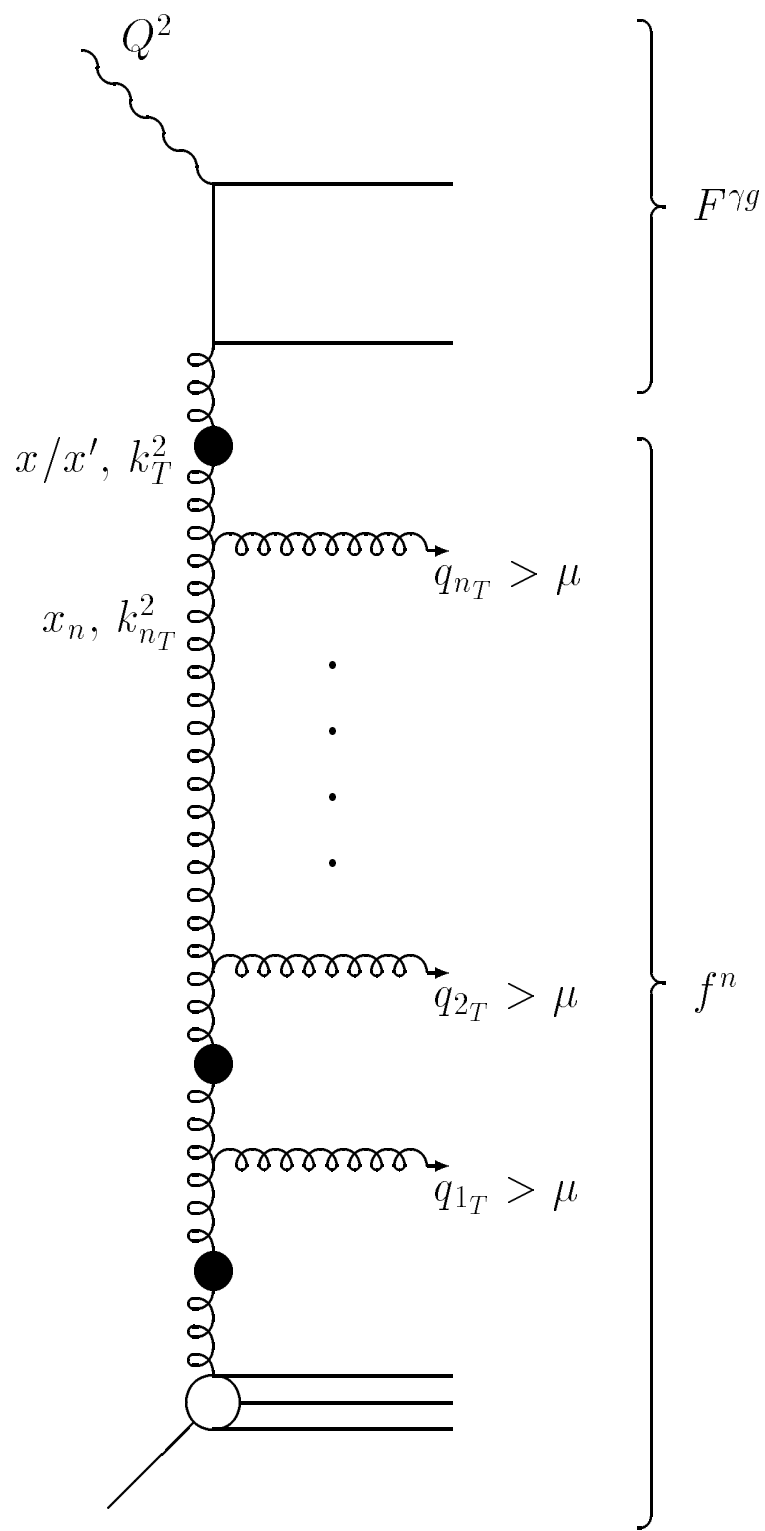


fig. 3

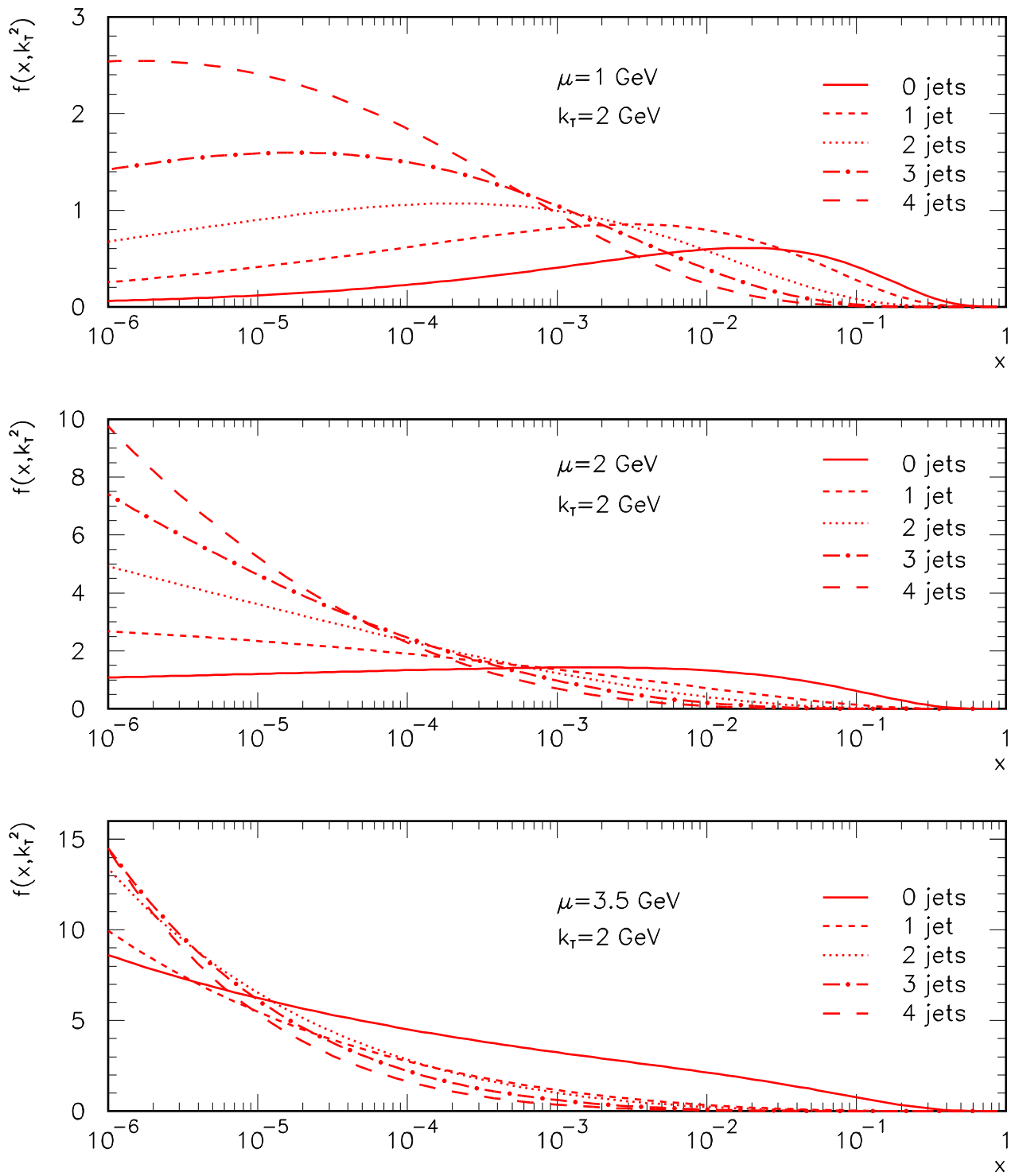


fig. 4

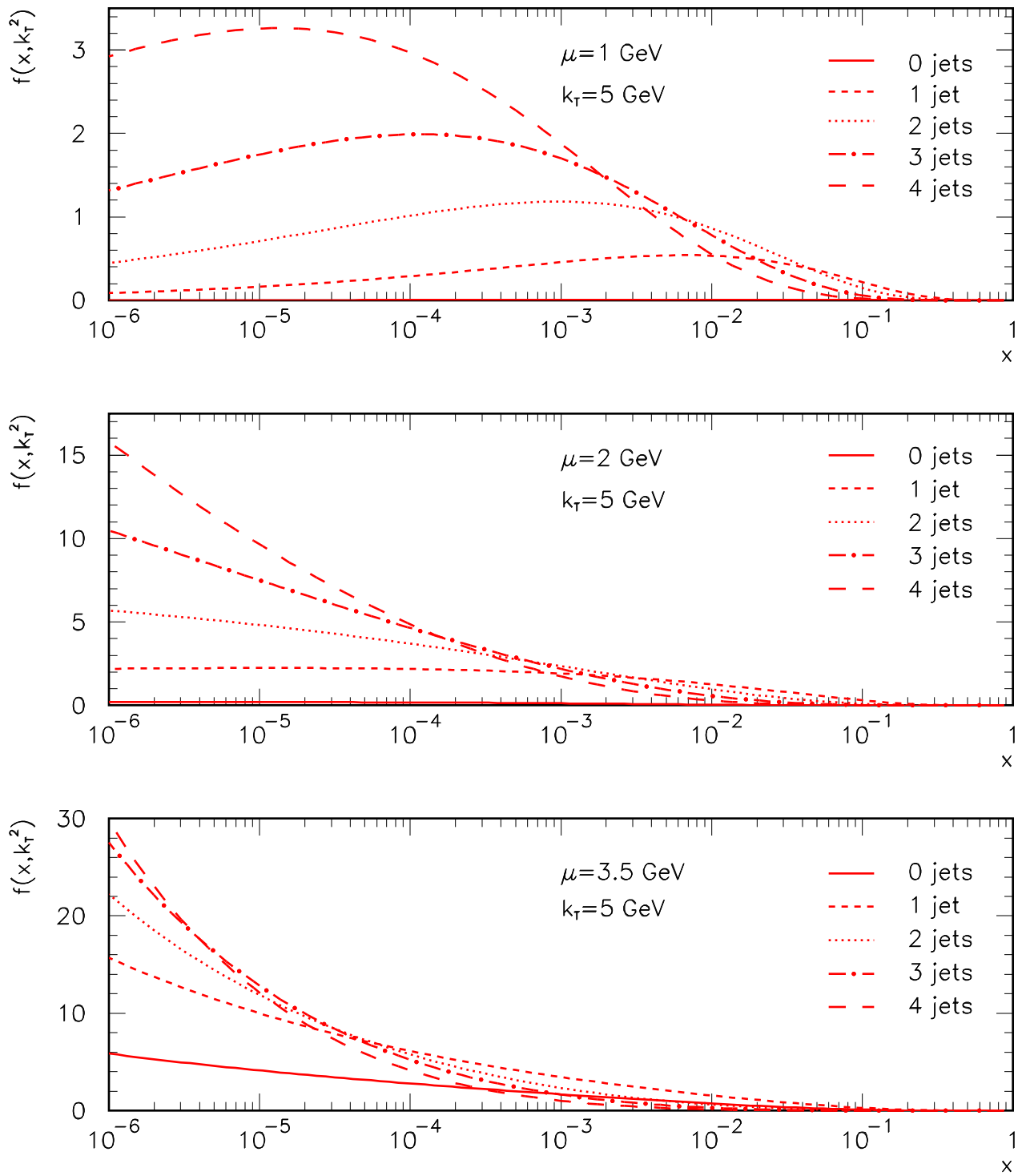


fig. 5

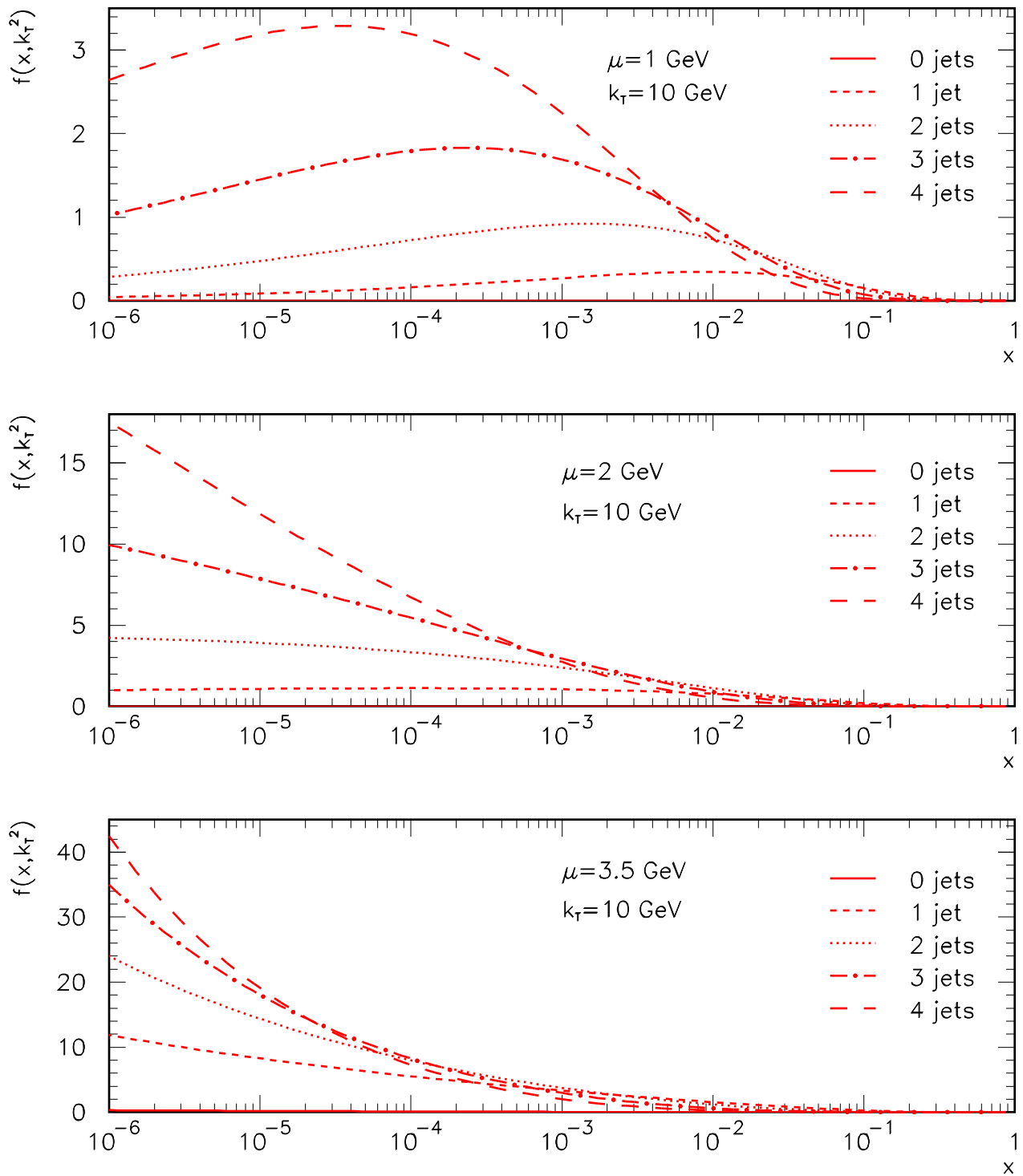


fig. 6

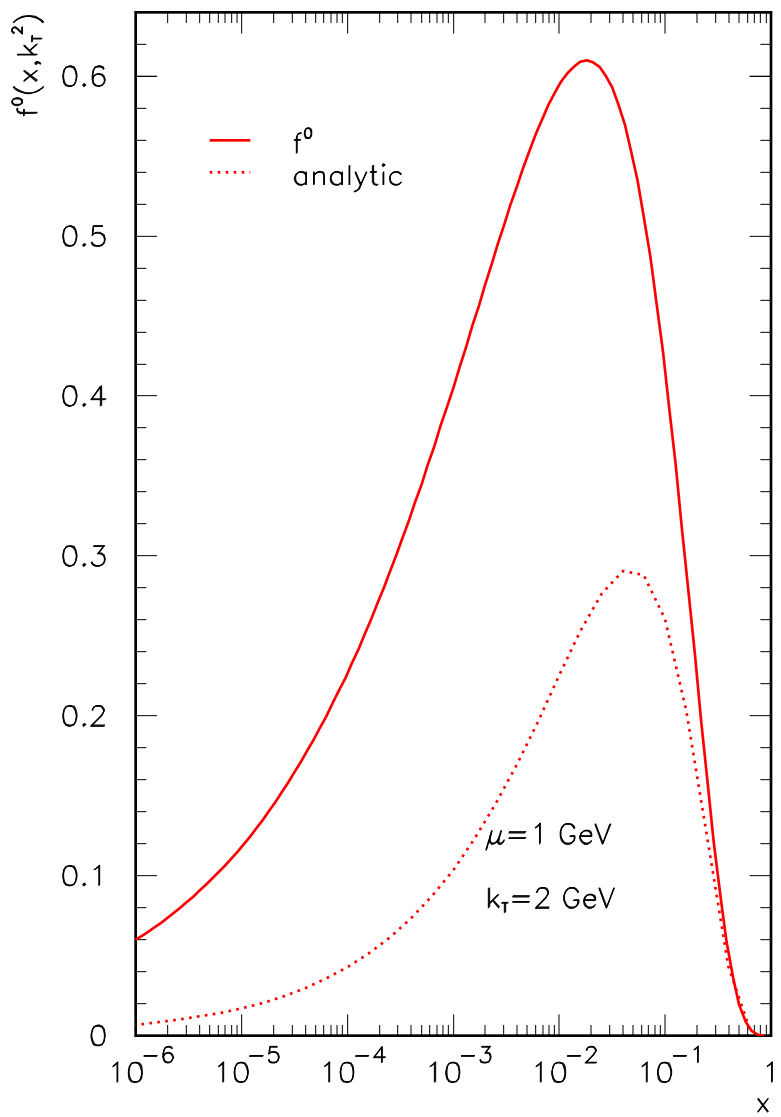


fig. 7

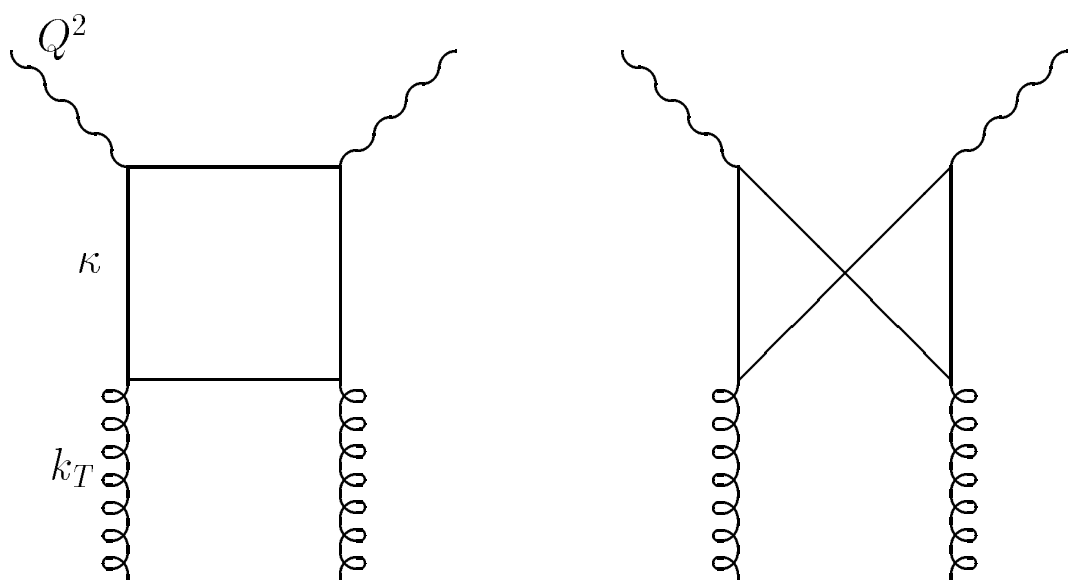


fig. 8

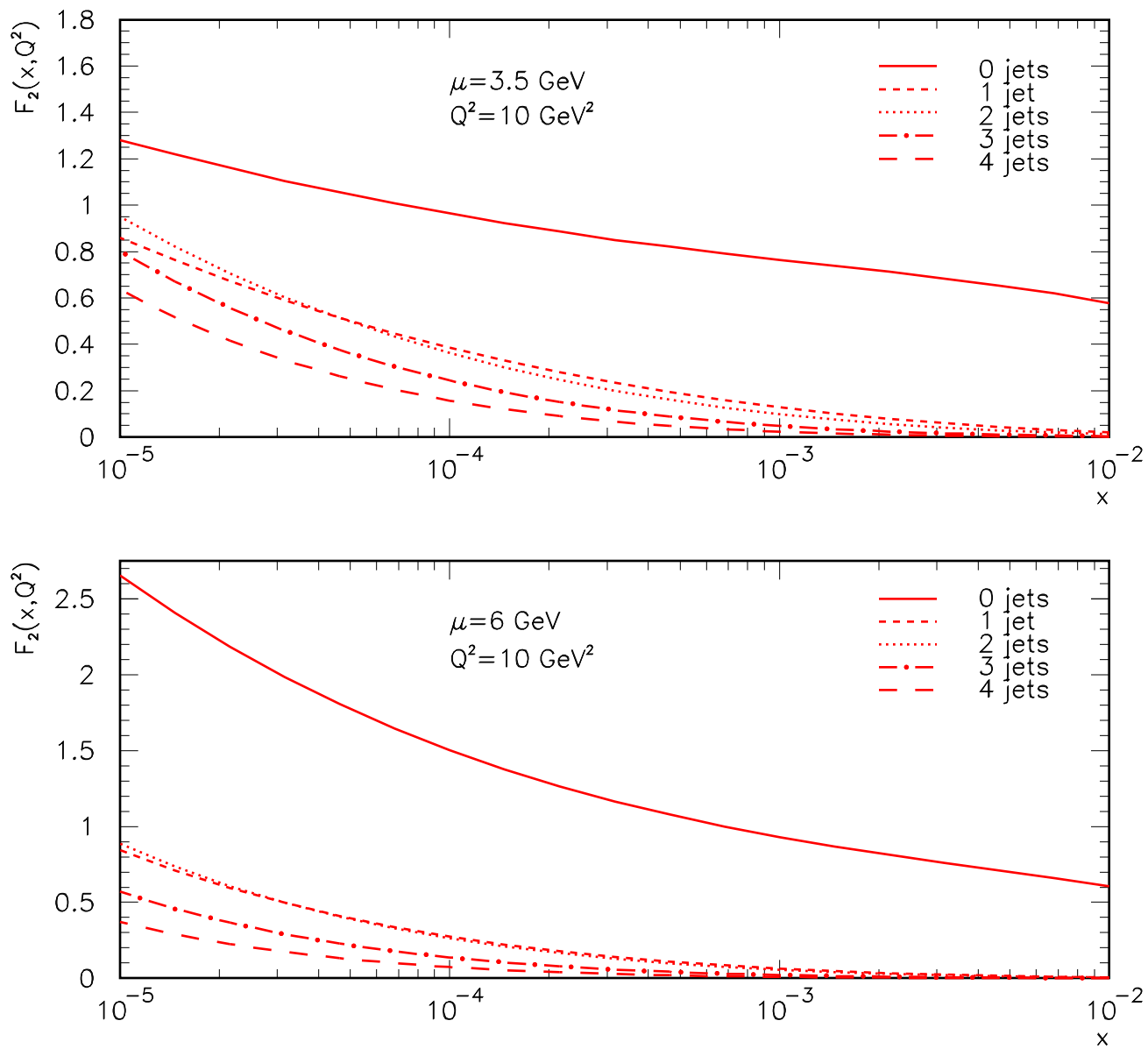


fig. 9

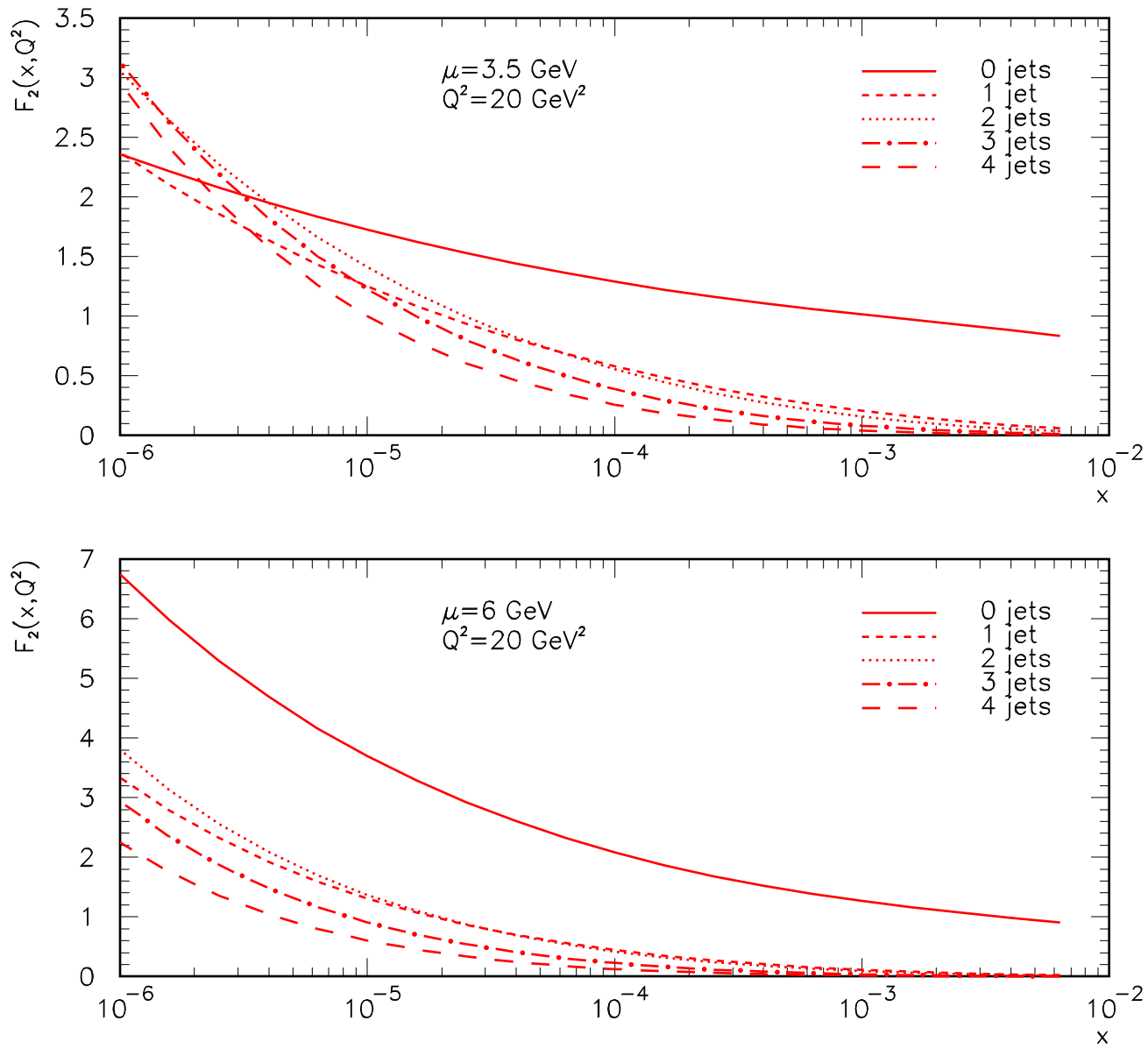


fig. 10

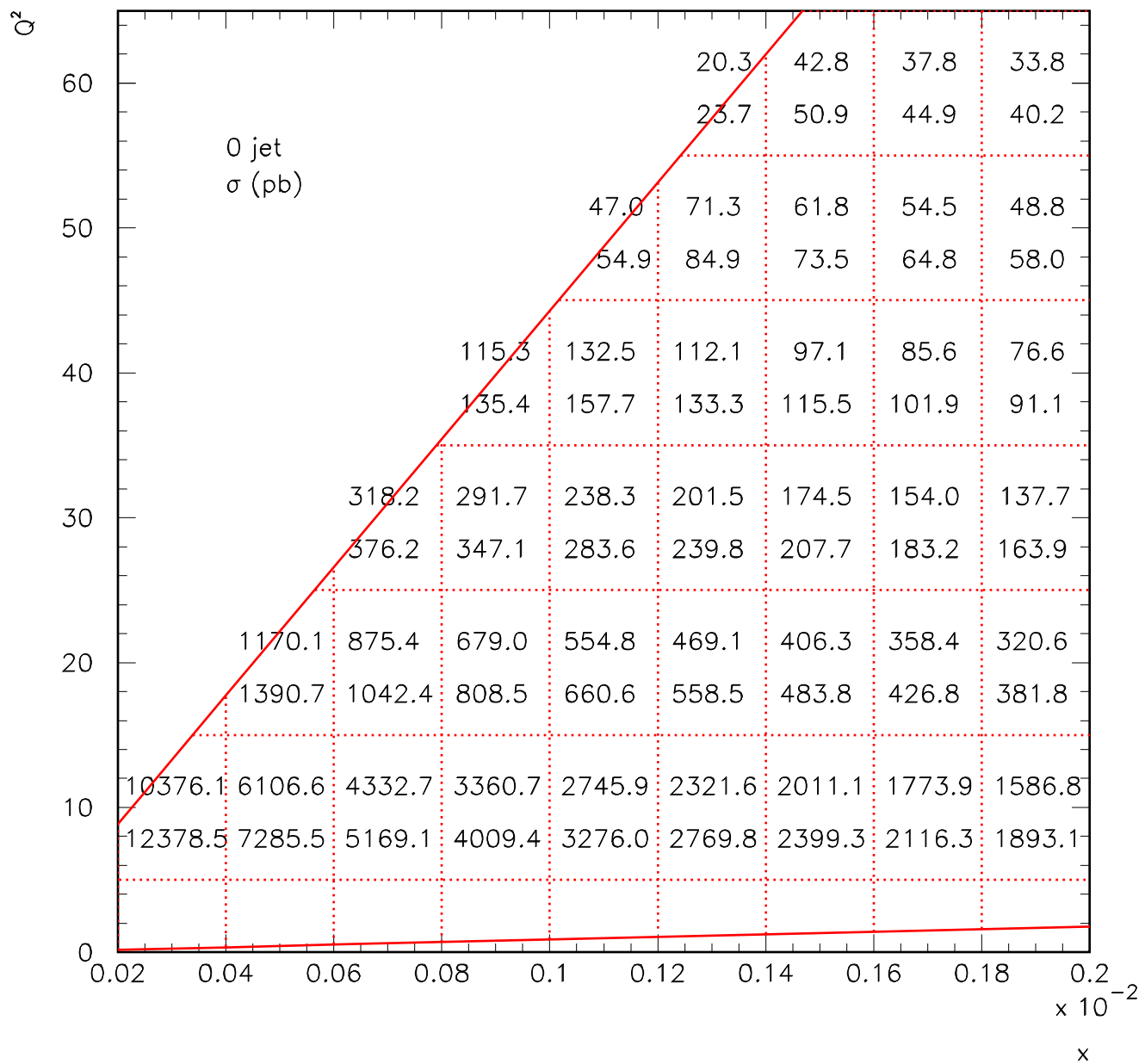


fig. 11

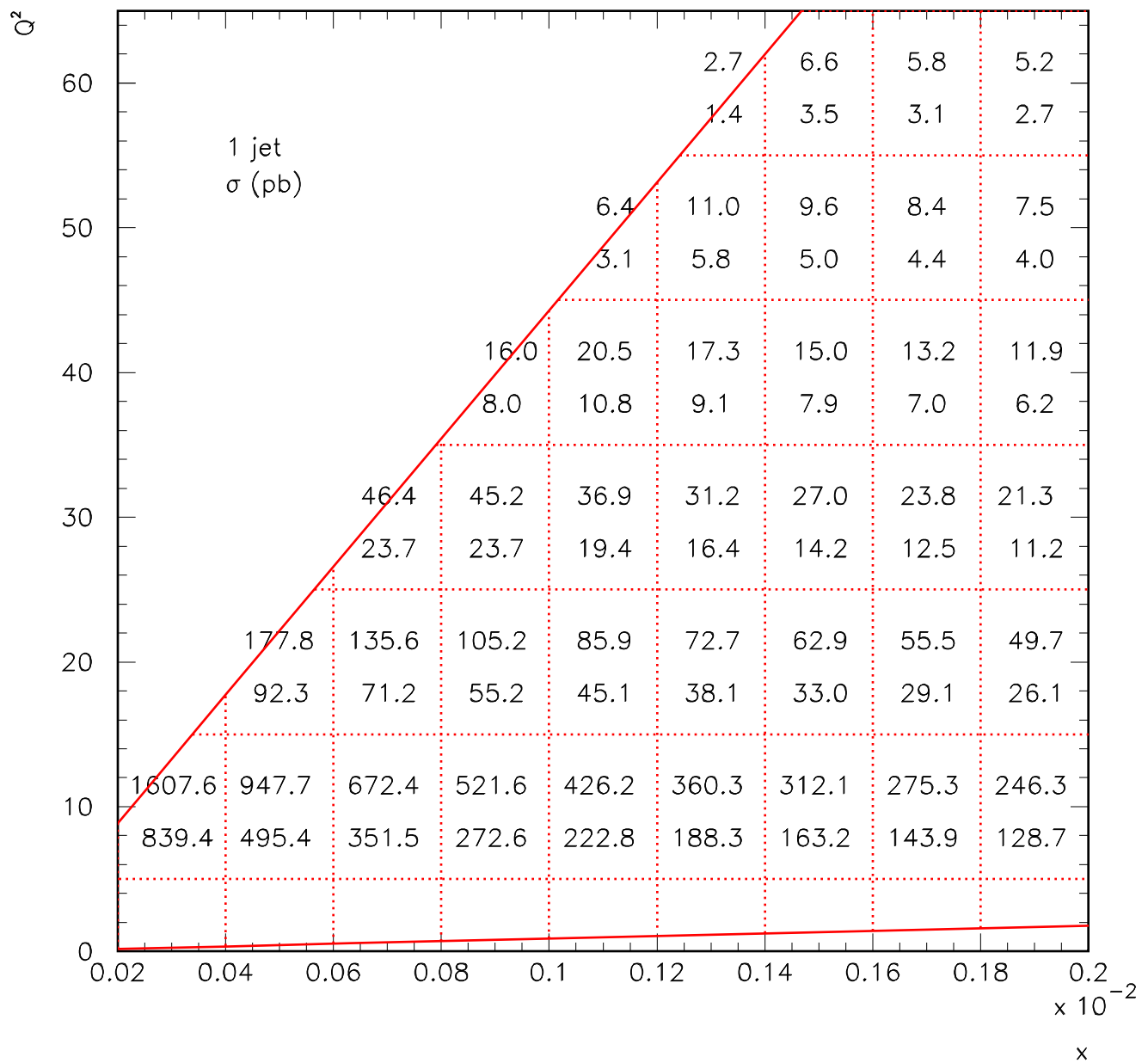


fig. 12

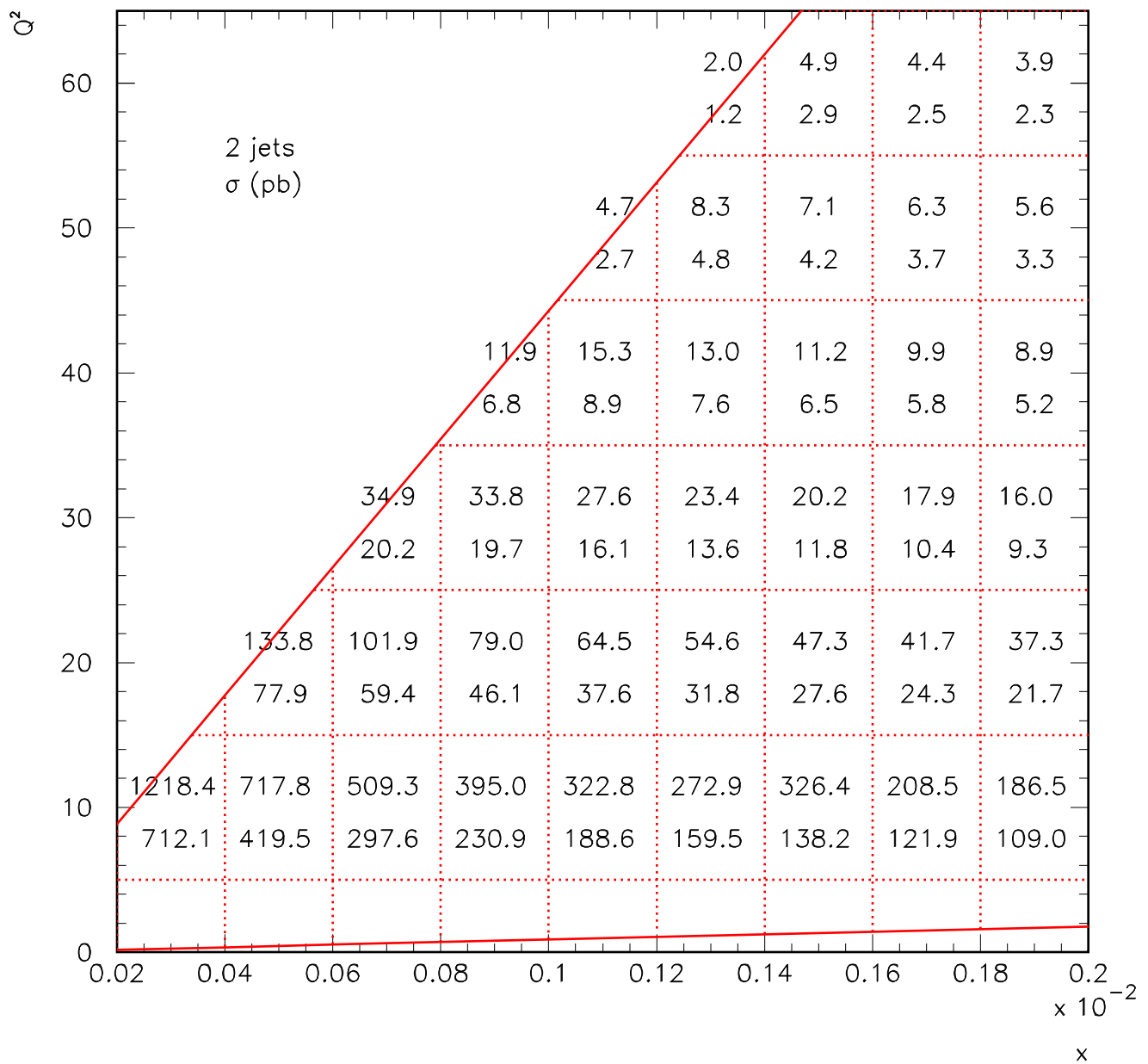


fig. 13

